Icarus 219 (2012) 13–24

Contents lists available at SciVerse ScienceDirect

Icarus

journal homepage: www.elsevier.com/locate/icarus

Chemical pathway analysis of the Martian atmosphere: CO_2-formation pathways

Joachim W. Stock [a,*], Christopher S. Boxe [b,f], Ralph Lehmann [c], J. Lee Grenfell [d], A. Beate C. Patzer [d], Heike Rauer [a,d], Yuk L. Yung [e]

[a] Institut für Planetenforschung, Deutsches Zentrum für Luft- und Raumfahrt (DLR), Rutherfordstr. 2, 12489 Berlin, Germany
[b] Earth and Space Science Division, Jet Propulsion Laboratory, California Institute of Technology, 4800 Oak Grove Drive, Pasadena, CA 91109, United States
[c] Alfred-Wegener-Institut für Polar- und Meeresforschung (AWI), Telegrafenberg A43, 14473 Potsdam, Germany
[d] Zentrum für Astronomie und Astrophysik (ZAA), Technische Universität Berlin (TUB), Hardenbergstr. 36, 10623 Berlin, Germany
[e] Division of Geological and Planetary Sciences, California Institute of Technology, 1200 East California Boulevard, Pasadena, CA 91125, United States
[f] Department of Physical, Environmental and Computer Science, Medgar Evers College-City University of New York, 1650 Bedford Avenue, Brooklyn, NY 11235, United States

ARTICLE INFO

Article history:
Received 19 October 2011
Revised 26 January 2012
Accepted 10 February 2012
Available online 22 February 2012

Keywords:
Atmospheres, Chemistry
Atmospheres, Composition
Mars
Mars, Atmosphere
Photochemistry

ABSTRACT

The chemical composition of a planetary atmosphere plays an important role for atmospheric structure, stability, and evolution. Potentially complex interactions between chemical species do not often allow for an easy understanding of the underlying chemical mechanisms governing the atmospheric composition. In particular, trace species can affect the abundance of major species by acting in catalytic cycles. On Mars, such cycles even control the abundance of its main atmospheric constituent CO_2. The identification of catalytic cycles (or more generally chemical pathways) by hand is quite demanding. Hence, the application of computer algorithms is beneficial in order to analyze complex chemical reaction networks. Here, we have performed the first automated quantified chemical pathways analysis of the Martian atmosphere with respect to CO_2-production in a *given* reaction system. For this, we applied the *Pathway Analysis Program* (PAP) to output data from the Caltech/JPL photochemical Mars model. All dominant chemical pathways directly related to the global CO_2-production have been quantified as a function of height up to 86 km. We quantitatively show that CO_2-production is dominated by chemical pathways involving HO_x and O_x. In addition, we find that NO_x in combination with HO_x and O_x exhibits a non-negligible contribution to CO_2-production, especially in Mars' lower atmosphere. This study reveals that only a small number of chemical pathways contribute significantly to the atmospheric abundance of CO_2 on Mars; their contributions to CO_2-production vary considerably with altitude. This analysis also endorses the importance of transport processes in governing CO_2-stability in the Martian atmosphere. Lastly, we identify a previously unknown chemical pathway involving HO_x, O_x, and HO_2-photodissociation, contributing 8% towards global CO_2-production by chemical pathways using recommended up-to-date values for reaction rate coefficients.

1. Introduction

One of the fundamental questions of planetary science concerns the photochemical stability of CO_2-dominated atmospheres in our Solar System, especially on Mars (95.32%, Owen et al., 1977). There, CO_2 is photolyzed by solar UV radiation

$$CO_2 + h\nu \rightarrow CO + O, \qquad (R_{27})$$

where atomic oxygen subsequently forms O_2. The termolecular formation reaction

$$CO + O + M \rightarrow CO_2 + M \qquad (R_{120})$$

is not fast enough to compensate for the effective CO_2-destruction by photolysis. If one takes only the reaction products into account, one would therefore expect an atmosphere rich in CO and O_2, in contradiction to observations. This suggests that other mechanisms stabilize the observed CO_2 content of the Martian atmosphere. A first step in understanding the persistence of CO_2 in the Martian atmosphere was taken by McElroy and Donahue (1972) and Parkinson and Hunten (1972), who proposed chemical pathways involving O_x and HO_x chemistry reproducing CO_2 from CO and O. These pathways can be understood as sets of chemical reactions, where molecules from the O_x-family (i.e. O and O_3) and the HO_x-family (i.e. H, OH, and HO_2) or the HO_x-family only, are acting as catalysts. This means that there is no net production or consumption of the catalyst species by the chemical pathways. Such chemical pathways can therefore provide efficient alternative routes for CO_2-production, even if the catalyst species are only present in trace amounts. Further improvements in photochemical models were made by the investigation of NO_x (e.g., Krasnopolsky, 1993; Nair et al., 1994), and heterogeneous chemistry on dust and ice cloud particles (e.g.,

* Corresponding author.
E-mail address: joachim.stock@dlr.de (J.W. Stock).

0019-1035/$ - see front matter © 2012 Elsevier Inc. All rights reserved.
doi:10.1016/j.icarus.2012.02.010

Anbar et al., 1993; Atreya and Gu, 1994; Krasnopolsky, 1993; Lefèvre et al., 2008).

Several methods have been applied in order to gain more insight about chemical reaction systems in general. A variety of powerful methods use sensitivity analysis (for reviews, see Rabitz et al., 1983; Saltelli et al., 2005; Turányi, 1990), which aim at understanding the effects of uncertainties (e.g. in chemical reaction rate coefficients) on the chemical system. However, it is not possible to construct chemical pathways by sensitivity analysis methods only. The identification of chemical pathways is in general a demanding task and their manual construction is only possible for pathological examples or specific problems as e.g. methane photo-oxidation in Earth's atmosphere (Johnston and Kinnison, 1998). Algorithms which take only stoichiometric information into account, were developed by e.g. Milner (1964), Clarke (1988), and Schuster and Schuster (1993). However, since these algorithms do not account for reaction rates (kinetic information), they cannot provide any quantitative information for individual chemical pathways. Therefore, using such methods it is not possible to determine, which chemical pathways dominate the reaction system. Moreover, these methods are usually not applicable to large reaction networks, because the number of pathways generally increases progressively with increasing number of reactions ("combinatorial explosion").

The algorithm used in this study (PAP – *Pathway Analysis Program*) takes stoichiometric as well as kinetic information (i.e. reaction rates) into account and is capable of identifying and quantifying all significant chemical pathways for a *given* chemical reaction system. Developed by Lehmann (2004), it has been applied to Earth's stratospheric ozone-chemistry (Lehmann, 2004; Grenfell et al., 2006), Earth's mesospheric ion-chemistry (Verronen et al., 2011), and Mars' near surface atmospheric chemistry (Stock et al., 2011).

However, quantification of all dominant chemical pathways forming CO_2 in the whole Martian atmosphere is still lacking. In order to determine the contributions of individual chemical pathways to the altitude-dependent CO_2-production, we apply the PAP algorithm to the results of the Caltech/JPL photochemical 1-D model of the Martian atmosphere. From this we derive the global mean CO_2-production by each of these pathways.

2. Method

2.1. Pathway Analysis Program (PAP)

2.1.1. The algorithm

The *Pathway Analysis Program* (Lehmann, 2004) enables the identification and quantification of chemical pathways in arbitrary *given* reaction systems. For this purpose, starting with individual reactions as pathways, longer pathways are formed step by step by connecting shorter pathways at so-called 'branching-point species'. At each step this branching-point species is chosen to be the species with the shortest lifetime with respect to the pathways formed in the previous steps. The algorithm terminates if a prescribed lifetime threshold $\tau_{\max}$ is reached or just before a prescribed species of interest S^* would become a branching-point species.

When a chemical species S_i is treated as a branching-point species, then each pathway producing S_i is connected with each pathway consuming S_i, in order to form a new longer pathway. A conservation of rates is valid, i.e. the sum of the rates of the new pathways "containing" a shorter pathway is equal to the rate of this shorter pathway. If the production and destruction rates of S_i are equal, the newly formed pathways recycle S_i completely, i.e. they are S_i-null-pathways. Otherwise, i.e. if there is a net concentration change of S_i, a fraction of the rate of each pathway producing S_i (in the case of a net production of S_i) or consuming S_i (in the case of a net consumption of S_i) remains after the connection of pathways. These pathways and their (remaining) rates become a part of the final result of the pathway analysis, explaining the net production or consumption of S_i.

Even if S_i has not been treated as a branching-point species, S_i-null-pathways may occur if the connection of pathways at a (shorter-lived) branching-point species $S_{i'}$ ($i' \neq i$) forms pathways which recycle not only $S_{i'}$ (by construction), but also S_i ("coincidentally").

In general, two problems can occur during the construction of chemical pathways when using a diagnostic algorithm. Firstly, the number of pathways can increase drastically with the number of reactions N_R and the number of species N_S due to "combinatorial explosion". To deal with this problem, the PAP algorithm possesses the capability to identify insignificant pathways at an early stage of the analysis (Lehmann, 2004). Such pathways are rejected if their rates are smaller than a prescribed threshold rate $f_{\min}$. If $f_{\min}$ is chosen to be too large, potentially important pathways would be deleted and the total production or consumption of the species of interest can not be completely explained by the pathways determined using the algorithm. On the other hand, if $f_{\min}$ is chosen too small, required computational time and memory increase rapidly. The effect of the choice of the parameter $f_{\min}$ on the analysis results for Martian near-surface atmospheric conditions was discussed by Stock et al. (2011). Secondly, chemical pathways can become unnecessarily complicated, e.g. containing null pathways as sub-pathways. In such cases the PAP algorithm splits the affected pathways into smaller ("elementary") subpathways by the method described by Schuster and Schuster (1993) and Lehmann (2004). A more detailed description of the PAP algorithm can be found in Lehmann (2004). Further details related to the application on Martian chemistry are given by Stock et al. (2011).

2.1.2. Required input quantities

In order to determine chemical pathways, stoichiometric and kinetic data from the results of a photochemical model are needed by the PAP algorithm. These are

(i) a complete list of N_S chemical species and N_R reactions of the chemical system, where $N_S \in \mathbb{N}$ and $N_R \in \mathbb{N}$ are the total number of species and the total number of reactions, respectively,

(ii) the concentrations averaged over a time interval $[0, \Delta t]$

$$\langle n_i \rangle(\boldsymbol{x}) := \frac{1}{\Delta t} \int_0^{\Delta t} n_i(\boldsymbol{x}, t) \mathrm{d}t, \quad i = 1, \ldots, N_S \tag{1}$$

of all species, where $n_i(\boldsymbol{x}, t)$ is the concentration of species S_i at location $\boldsymbol{x}$ and time t,

(iii) the time-averaged reaction rates

$$\langle r_j \rangle(\boldsymbol{x}) := \frac{1}{\Delta t} \int_0^{\Delta t} r_j(\boldsymbol{x}, t)\ \mathrm{d}t, \quad j = 1, \ldots, N_R \tag{2}$$

of all reactions, where $r_j(\boldsymbol{x}, t)$ denotes the reaction rate of reaction R_j at location $\boldsymbol{x}$ and time t, and

(iv) the concentration changes

$$\Delta n_i(\boldsymbol{x}) = \sum_{j=1}^{N_R} s_{ij} \langle r_j \rangle(\boldsymbol{x})\ \Delta t, \quad i = 1, \ldots, N_S \tag{3}$$

caused by chemical reactions during the time interval $[0, \Delta t]$ for all species S_i located at $\boldsymbol{x}$, where $s_{ij} \in \mathbb{Z}$ are the components of the stoichiometric matrix.

2.2. Definitions

In this paper we will make use of the following definitions. In accordance with Lehmann (2004), we denote the stoichiometric coefficients of the net reaction of a pathway P_k with m_{ik} ($m_{ik} \in \mathbb{Z}$). These coefficients m_{ik} are related to the stoichiometric coefficients s_{ij} of the individual reactions by

$$m_{ik} = \sum_{j=1}^{N_R} s_{ij}\lambda_{jk}, \quad i = 1,\ldots,N_S, \;\; k = 1,\ldots,N_P, \tag{4}$$

where $\lambda_{jk} \in \mathbb{N} \cup \{0\}$ is the multiplicity of reaction R_j in pathway P_k and $N_P \in \mathbb{N}$ the total number of chemical pathways. Additionally, we denote the mean rate of a pathway P_k in the time interval $[0, \Delta t]$ with f_k. The rates of all reactions R_j are completely distributed to the chemical pathways P_k, therefore the following relation holds:

$$\langle r_j \rangle = \sum_{k=1}^{N_P} \lambda_{jk} f_k, \quad j = 1,\ldots,N_R. \tag{5}$$

Since all summands in Eq. (5) are non-negative, we obtain for each of them

$$\lambda_{jk} f_k \leqslant \langle r_j \rangle, \quad j = 1,\ldots,N_R, \;\; k = 1,\ldots,N_P. \tag{6}$$

If $\lambda_{jk} \neq 0$, it follows:

$$f_k \leqslant \frac{\langle r_j \rangle}{\lambda_{jk}}, \quad j = 1,\ldots,N_R, \;\; k = 1,\ldots,N_P. \tag{7}$$

Consequently, the rate of pathway P_k cannot exceed

$$f_k^{\max} := \min\left\{ \frac{\langle r_j \rangle}{\lambda_{jk}} \,\middle|\, \lambda_{jk} \neq 0, \; j \in \{1,\ldots,N_R\} \right\}. \tag{8}$$

The rate of the net change of species S_i by pathway P_k can be defined as

$$\varphi_{ik} := |m_{ik}| f_k, \quad i = 1,\ldots,N_S, \;\; k = 1,\ldots,N_P. \tag{9}$$

From Eqs. (7) and (9) it immediately follows that

$$\varphi_{ik} \leqslant |m_{ik}| \frac{\langle r_j \rangle}{\lambda_{jk}}, \quad i = 1,\ldots,N_S, \;\; k = 1,\ldots,N_P,$$
$$\forall j \in \{1,\ldots,N_R\} : \lambda_{jk} \neq 0. \tag{10}$$

This means that the rate of the net change of species S_i by pathway P_k is constrained by

$$\rho_{ijk} := \frac{|m_{ik}|}{\lambda_{jk}} \langle r_j \rangle \tag{11}$$

for each reaction R_j in pathway P_k.

2.3. Photochemical column model

To obtain the required data to perform the pathway analysis of the Martian atmospheric chemistry, the reaction rate network equations

$$\frac{\partial}{\partial t} n_i(\boldsymbol{x}, t) + \operatorname{div} \boldsymbol{\Phi}_i(\boldsymbol{x}, t) = \mathcal{P}_i(n_1,\ldots,n_{N_S}) - \mathcal{L}_i(n_1,\ldots,n_{N_S}), \tag{12}$$

have to be solved, where $\mathcal{P}_i(n_1,\ldots,n_{N_S})$ denotes the total production rate of species S_i by all chemical reactions and $\mathcal{L}_i(n_1,\ldots,n_{N_S})$ the total loss rate by all chemical reactions, respectively. Here, we assume stationary conditions (i.e. $\partial n_i/\partial t = 0$) and a plane-parallel geometry, where z denotes the altitude. The vertical flux of species S_i can then be described by

$$\boldsymbol{\Phi}_i = -D_i\left(\frac{\mathrm{d}n_i}{\mathrm{d}z} + \frac{n_i}{H_i} + \frac{n_i(1+\alpha_i)}{T}\frac{\mathrm{d}T}{\mathrm{d}z}\right) - K\left(\frac{\mathrm{d}n_i}{\mathrm{d}z} + \frac{n_i}{H} + \frac{n_i}{T}\frac{\mathrm{d}T}{\mathrm{d}z}\right), \tag{13}$$

where D_i is the molecular diffusion coefficient, H_i the scale height, and α_i the thermal diffusion factor of species S_i. K denotes the eddy diffusion coefficient and H the scale height of the background atmosphere.

We utilize the Caltech/JPL one-dimensional photochemical kinetics model for a latitude of 30° at equinox. This model is an update of the Nair et al. (1994) model. It is similar to that used by Yung et al. (1988) and Nair et al. (1994) to study the, overall, photochemical state of the Martian atmosphere. A detailed description of the 1-D photochemical model is given by Nair et al. (1994); we, therefore, only provide a short description of the model. Specifically, it incorporates Mars atmospheric oxygen, carbon, hydrogen, and nitrogen chemistry in the presence of vertical diffusive transport and allows for time-dependent calculations. It solves the 1-D continuity equation

$$\frac{\partial}{\partial t} n_i(z,t) + \frac{\partial}{\partial z} \boldsymbol{\Phi}_i(z,t) = \mathcal{P}_i(n_1,\ldots,n_{N_S}) - \mathcal{L}_i(n_1,\ldots,n_{N_S}), \tag{14}$$

for 27 species (O, O(^{1}D), O_2, O_3, N, N(^{2}D), N_2, N_2O, NO, NO_2, NO_3, N_2O_5, HNO_2, HNO_3, HO_2NO_2, H, H_2, H_2O, OH, HO_2, H_2O_2, CO, CO_2, O^+, O_2^+, CO_2^+, and CO_2H^+) in 126 reactions (see Appendix A) from the surface to the exosphere at 240 km (with 2 km resolution) in 121 levels. All reaction rate coefficients were updated according to Sander et al. (2006); diurnally-averaged values of them are used. The steady-state is considered to be reached when the volume mixing ratio changes of all species are less than 0.01% in the final time step (4.89×10^{29} s). The vertical flux is given by Eq. (13). The thermal diffusion factor α_i is set to be zero for all species S_i throughout our calculations.

2.4. Application: Martian atmosphere

For the chemical pathways analysis, the PAP algorithm is applied to the steady-state solution of the Caltech/JPL column model for each vertical layer separately. Due to the assumptions made, Eqs. (1) and (2) simply reduce to

$$\langle n_i \rangle(z) = n_i(z), \quad i = 1,\ldots,N_S \tag{15}$$

and

$$\langle r_j \rangle(z) = r_j(z), \quad j = 1,\ldots,N_R, \tag{16}$$

respectively. The concentration changes $\Delta n_i(z)$ caused solely by chemical reactions are obtained from Eq. (3). Although we have assumed steady-state, these concentrations changes $\Delta n_i(z)$ are not necessarily zero, because of the divergence of the vertical flux $\partial \Phi_i(z)/\partial z$ (see Eq. (14)). Since $\Delta n_i(z)$ scales linearly with Δt for stationary conditions, the specific choice of the time-interval Δt does not affect the analysis results.

In order to determine the pathways responsible for the budget of the carbon-bearing species CO and CO_2, we applied the PAP algorithm, such that the species of interest mentioned in Section 2.1.1 are CO and CO_2. As described there, the choice of the branching-point species depends on their chemical lifetime. Since the chemical lifetime of a species S_i generally varies with altitude, it may happen that some species are considered as branching-point species only for a limited range of altitude. The threshold rate $f_{\min}$ (see Section 2.1.1) is chosen to be $f_{\min} = 10^{-8}$ ppb h^{-1} (see Stock et al. (2011) for discussion). With this choice, more than 99.983% of the total CO_2-production by chemical pathways is identified by the PAP algorithm in each vertical layer.

The globally-averaged relative contribution to the production q_{ik} of a species S_i by a chemical pathway P_k is calculated by

$$q_{ik} = \frac{\int_0^{\Delta z} \varphi_{ik}(z)\mathrm{d}z}{\int_0^{\Delta z} \sum\limits_{\{l|m_{il}>0\}} \varphi_{il}(z)\mathrm{d}z}, \quad \forall k \in \{1,\ldots,N_P\} : m_{ik} > 0, \tag{17}$$

where $\varphi_{ik}(z)$ is defined in Eq. (9) and Δz is the extent of the atmosphere of interest. The value of Δz is set to 86 km for our analysis, because the major fraction of the global CO_2 production takes place below this level and proceeds via neutral chemistry (cf. Fig. 1). The error ε_i caused by integrating only up to Δz = 86 km is estimated to be

$$\varepsilon_i = 1 - \frac{\int_0^{\Delta z} \sum_{\{k|m_{ik}>0\}} \varphi_{ik}(z)\mathrm{d}z\Big|_{\Delta z=86\mathrm{km}}}{\int_0^{\Delta z} \sum_{\{k|m_{ik}>0\}} \varphi_{ik}(z)\mathrm{d}z\Big|_{\Delta z=240\mathrm{km}}} = 3.7\times10^{-5},$$

$$S_i = \mathrm{CO_2}, \tag{18}$$

where the upper boundary of the photochemical model is located at 240 km. The small value of ε_i mainly results from the exponential decrease of the density with altitude. Note, that the scale height is H = 11.1 km at the Martian surface (Yung and DeMore, 1999). Thus, the choice of Δz = 86 km is sufficient for the purposes of this study.

3. Results and discussion

Fig. 1 shows the total CO_2-production and loss rate due to all chemical reactions. The production rate profile indicates, that there are two different chemical regimes in the Martian atmosphere. In the lower part of the atmosphere, i.e. z < 86 km, CO_2 is mainly formed from CO via

$$\mathrm{CO + OH \rightarrow CO_2 + H.} \tag{R123}$$

In the upper region of the atmosphere (z > 86 km) ionic chemistry becomes important. Here, CO_2 is mainly formed from CO_2^+ by charge-exchange ionization

$$\mathrm{CO_2^+ + O \rightarrow CO_2 + O^+.} \tag{R125}$$

The destruction of CO_2 takes place mainly due to the photo-dissociation which yields CO via reaction R_{27}. Fig. 1 also illustrates that the modeled Martian atmosphere is not in kinetic equilibrium because the production rate $\mathcal{P}_{CO_2}(z)$ and loss rate $\mathcal{L}_{CO_2}(z)$ are not equal for each altitude. For higher altitudes (z > 43 km) CO_2 is effectively destroyed, whereas for lower altitudes (z < 43 km) CO_2 is effectively produced. Therefore, Fig. 2 shows a decrease in the volume mixing ratio of CO_2 and an increase in the volume mixing ratio of CO with altitude. This leads to an upward CO_2 flux accompanied by a downward CO flux due to (eddy-)diffusion (see Eq. (13)). The column

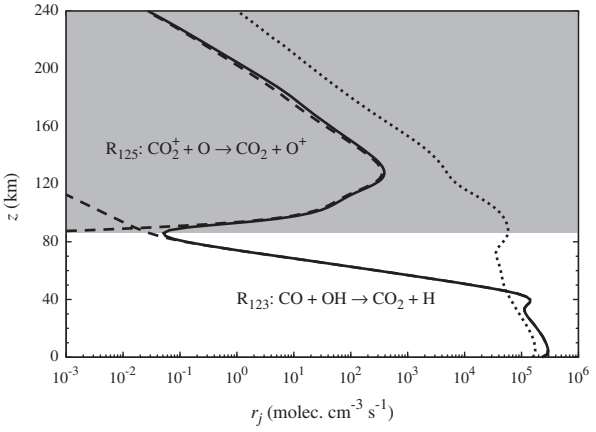

Fig. 1. CO_2-production rates. Total CO_2-production rate $\mathcal{P}_{CO_2}(z)$ (solid line) and total destruction rate $\mathcal{L}_{CO_2}(z)$ (dotted line) by all chemical reactions. Dashed curves indicate the rates of the reactions with the largest contributions to the total CO_2-production.

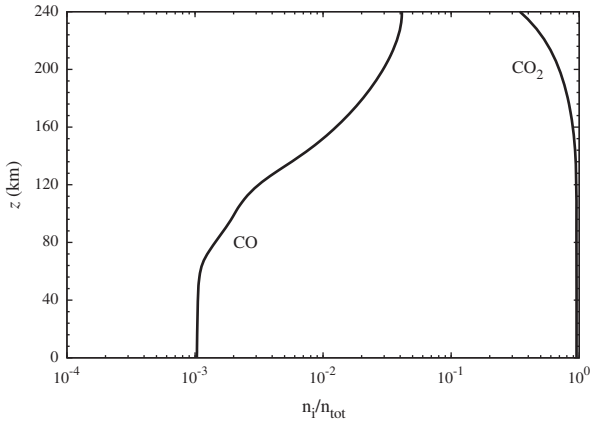

Fig. 2. Modeled CO and CO_2 volume mixing ratio altitude profiles. n_{tot} denotes the total number density of the atmosphere at given altitude.

integrated values of $\mathcal{P}_{CO_2}(z)$ and $\mathcal{L}_{CO_2}(z)$, however, are equal within the numerical uncertainty. Consequently, the Martian atmosphere is in this context chemically stable according to the model results. Since CO_2-production occurs mostly in the lower layers, we will focus our analysis on this part of the atmosphere.

The production rate of a species S_i by the sum of all chemical reactions which produce it (as in Fig. 1) is larger than or equal to the production rate by all S_i producing chemical pathways (Fig. 3), because a fraction of the S_i producing reaction rate may be distributed to S_i-null-pathways (cf. Section 2.1.1). An example of a CO_2-null-pathway is pathway P_{14}. In the following, the term CO_2-production corresponds to the CO_2-production by CO_2-non-null-pathways. In order to discuss the CO_2-production-pathways found by the PAP algorithm, it is convenient to group certain species into chemical families termed: HO_x (=H + OH + HO_2), O_x (=O + O_3), and NO_x = NO + NO_2). This convention results in three classes of dominant pathways in our chemical reaction system, which can be further divided into smaller (sub-)groups according to specific reactions (see Table 1). In Fig. 3 the contributions of the most efficient pathways are shown. Each of the nine dominant pathways has at least 3% contribution to the total CO_2-production by chemical pathways in one or more layers up to $z \leqslant 86$ km. The dominant pathways, presented in this study, account for 96.6% of CO_2-production. The remaining 3.4% are due to a large number of chemical pathways that individually contribute a minor fraction to the CO_2-production. This is due to an increasing mixing ratio of NO_x in the lower part of the atmosphere, which leads to higher reaction rates of NO_x-involving reactions and therefore a larger efficiency of O_x–HO_x–NO_x-pathways.

3.1. Class I: O_x–HO_x-pathways

The O_x–HO_x-pathways in Tables 2 and 3 (P_1–P_6) found in this study can be further split into two sub-groups, depending on

Table 1
Classification of CO_2-production-pathways in this paper. The first row lists the nine dominant CO_2-production-pathways. In the first column the families are shown. A bullet (•) indicates that a molecule from the family is participating in the given pathway. The last row denotes the pathway class.

	P_1	P_2	P_3	P_4	P_5	P_6	P_7	P_8	P_9
O_x	•	•	•	•	•	•			•
HO_x	•	•	•	•	•	•	•	•	•
NO_x									•
Class	Ia				Ib		II		III

Table 2
Class Ia O_x–HO_x-pathway percentage-contribution to the global CO_2-production by all CO_2-production-pathways. Values on the right hand side are calculated according to Eq. (17).

P_1	$O_2 + h\nu \rightarrow O + O$ $2 \cdot (O + HO_2 \rightarrow OH + O_2)$ $2 \cdot (CO + OH \rightarrow CO_2 + H)$ $2 \cdot (H + O_2 + M \rightarrow HO_2 + M)$	
net:	$2CO + O_2 \rightarrow 2CO_2$	**40.2%**
P_2	$O + HO_2 \rightarrow OH + O_2$ $CO + OH \rightarrow CO_2 + H$ $H + O_2 + M \rightarrow HO_2 + M$	
net:	$CO + O \rightarrow CO_2$	**18.5%**
P_3	$HO_2 + h\nu \rightarrow OH + O$ $O + HO_2 \rightarrow OH + O_2$ $2 \cdot (CO + OH \rightarrow CO_2 + H)$ $2 \cdot (H + O_2 + M \rightarrow HO_2 + M)$	
net:	$2CO + O_2 \rightarrow 2CO_2$	**7.9%**
P_4	$O_3 + h\nu \rightarrow O_2 + O$ $O + HO_2 \rightarrow OH + O_2$ $CO + OH \rightarrow CO_2 + H$ $H + O_2 + M \rightarrow HO_2 + M$	
net:	$CO + O_3 \rightarrow CO_2 + O_2$	**2.1%**

Table 3
Class Ib O_x–HO_x-pathway percentage-contribution to the global CO_2-production by all CO_2-production-pathways. Values on the right hand side hand side are calculated according to Eq. (17).

P_5	$O + O_2 + CO_2 \rightarrow O_3 + CO_2$ $H + O_3 \rightarrow OH + O_2$ $CO + OH \rightarrow CO_2 + H$	
net:	$CO + O \rightarrow CO_2$	**6.3%**
P_6	$O_2 + h\nu \rightarrow O + O$ $2 \cdot (O + O_2 + CO_2 \rightarrow O_3 + CO_2)$ $2 \cdot (H + O_3 \rightarrow OH + O_2)$ $2 \cdot (CO + OH \rightarrow CO_2 + H)$	
net:	$2CO + O_2 \rightarrow 2CO_2$	**1.6%**

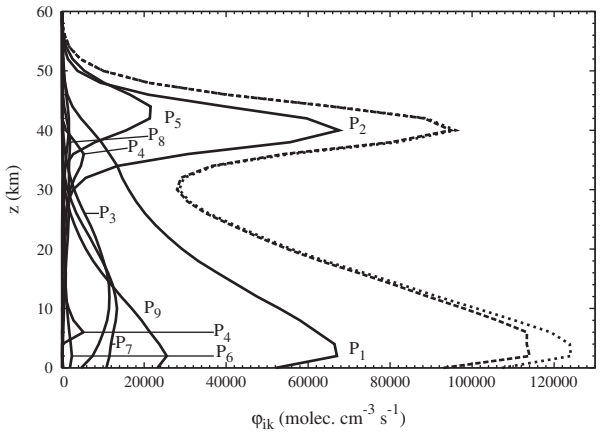

Fig. 3. Rate of the net change of CO_2 via CO_2-production-pathways. Solid lines indicate the contribution of the nine dominant pathways. The dotted line represents the total production of CO_2 by all CO_2-production-pathways. The dashed line is the sum of the contribution of the nine dominant pathways.

how H is transformed into OH. This proceeds either via the reaction with O_2 (sub-class Ia)

$$H + O_2 + M \rightarrow HO_2 + M, \quad (R_{47})$$

$$O + HO_2 \rightarrow OH + O_2, \quad (R_{67})$$

or via reaction with O_3 (sub-class Ib)

$$H + O_3 \rightarrow OH + O_2. \quad (R_{52})$$

3.1.1. Class Ia

Three of the pathways shown in Table 2 (P_1,P_2,P_4) are variations of the chemical scheme presented by McElroy and Donahue (1972). Since atomic oxygen has a short chemical lifetime in the lower part of the atmosphere relevant for CO_2-production, the PAP algorithm identifies it as a branching-point species. The atomic oxygen originates chemically mostly from either photolysis of molecular oxygen (P_1) or photolysis of ozone (P_4). Alternatively, atomic oxygen can be supplied by vertical transport due to eddy-diffusion (P_2). There is also the possibility to provide atomic oxygen via the photo-dissociation of CO_2 (reaction R_{27}). However, this will result in null pathways, which are neither producing nor consuming CO_2.

The rates of the production pathways $f_k(z)$ are naturally bounded from above by $f_k^{\max}(z)$ (see Section 2.2). However, in several cases this bound is not reached over wide altitude ranges as a result of competition with other chemical pathways (see Fig. 4a or Fig. 6b for example). In the following, we will therefore investigate the competing pathways in order to elucidate the interactions within the reaction network, when necessary.

Fig. 4a suggests that pathway P_1 is most efficient at $z = 4$ km and has the largest contribution to the global CO_2-production of all pathways identified in this study. Above $z = 4$ km its rate decreases monotonically with altitude. This is mainly due to the decrease of the reaction rate $r_1(z)$ of the O_2-photolysis reaction

$$O_2 + h\nu \rightarrow O + O, \quad (R_1)$$

which limits the rate $f_1(z)$ of the pathway P_1 between $z = 12$ km and $z = 34$ km. This effect results from the decrease of O_2 concentration with increasing altitude. However, not all atomic oxygen produced by reaction R_1 is consumed by P_1 (Fig. 4a). In order to investigate the fate of atomic oxygen produced by reaction R_1 between $z = 0$ km and $z = 12$ km (lower regime) as well as $z = 34$ km and $z = 51$ km (upper regime), we use PAP to find all pathways which include reaction R_1.

In the lower regime atomic oxygen produced by O_2-photolysis (reaction R_1) and not consumed by P_1 is primarily used for CO_2-production by pathways such as P_6 or the following:

$$\begin{aligned} &O_2 + h\nu \rightarrow O + O \\ &2 \cdot (O + NO_2 \rightarrow NO + O_2) \\ &2 \cdot (HO_2 + NO \rightarrow NO_2 + OH) \\ &2 \cdot (CO + OH \rightarrow CO_2 + H) \\ &2 \cdot (H + O_2 + M \rightarrow HO_2 + M) \\ &\text{net}: \quad O_2 + 2CO \rightarrow 2CO_2. \end{aligned} \quad (P_{10})$$

The pathways with the largest rates found by this search in the upper regime (Fig. 4a) are beside P_1 the null pathways

$$\begin{aligned} &O_2 + h\nu \rightarrow O + O \\ &O + HO_2 \rightarrow OH + O_2 \\ &O + OH \rightarrow O_2 + H \\ &H + O_2 + M \rightarrow HO_2 + M \\ &\text{net}: \quad \text{null}, \end{aligned} \quad (P_{11})$$

and

$$\begin{aligned} &O_2 + h\nu \rightarrow O + O \\ &O + OH \rightarrow O_2 + H \\ &O + O_2 + CO_2 \rightarrow O_3 + CO_2 \\ &H + O_3 \rightarrow OH + O_2 \\ &\text{net}: \quad \text{null}. \end{aligned} \quad (P_{12})$$

Since above $z = 51$ km the rate of P_1 cannot exceed the half of the reaction rate of the CO_2-forming reaction R_{123}, which also determines $f_1^{max}(z)$ in this region, one might also be interested in the fate of atomic hydrogen produced by reaction R_{123}. Only a small fraction of atomic hydrogen is here recycled by P_1. The majority of atomic hydrogen produced by reaction R_{123} is either consumed by the CO_2-production-pathways P_5 and P_2, or by the null pathways

$$\begin{aligned} &CO_2 + h\nu \rightarrow CO + O \\ &O + O_2 + CO_2 \rightarrow O_3 + CO_2 \\ &H + O_3 \rightarrow OH + O_2 \\ &CO + OH \rightarrow CO_2 + H \\ &\text{net :} \quad \text{null}, \end{aligned} \tag{P$_{13}$}$$

and

$$\begin{aligned} &CO_2 + h\nu \rightarrow CO + O \\ &O + HO_2 \rightarrow OH + O_2 \\ &H + O_2 + M \rightarrow HO_2 + M \\ &CO + OH \rightarrow CO_2 + H \\ &\text{net :} \quad \text{null}. \end{aligned} \tag{P$_{14}$}$$

At altitudes 34 km < z < 48 km CO_2-production is dominated by pathway P_2 (Fig. 3). In this part of the atmosphere, atomic oxygen is supplied by downward transport. Eq. (8) can be modified by treating transport processes of species S_i with $\tau_i < \tau_{max}$ or $\tau_i < \tau_*$ as pseudo reactions, where τ_* is the lifetime of S^* (cf. Section 2.1.1). Therefore the oxygen flux divergence is an upper bound to the rate of P_2 up to $z = 40$ km (Fig. 4b). The atomic oxygen, which is vertically transported and not consumed by pathway P_2 forms O_2 via

$$\begin{aligned} &O + HO_2 \rightarrow OH + O_2 \\ &O + OH \rightarrow O_2 + H \\ &H + O_2 + M \rightarrow HO_2 + M \\ &\text{net :} \quad 2O \rightarrow O_2, \end{aligned} \tag{P$_{15}$}$$

or CO_2 by pathway P_5. Above this altitude range, $f_2^{max}(z)$ is determined by the CO_2-formation reaction R_{123}. The atomic hydrogen produced by this reaction and not consumed by pathway P_2 is used by the CO_2-production-pathway P_5 and the null pathway P_{14}.

Here, we present for the first time a newly identified chemical CO_2-production-pathway – i.e. P_3 (see Table 2 and Fig. 4c), which accounts for ~8% of the total CO_2-production. It is characterized by HO_2 photolysis

$$HO_2 + h\nu \rightarrow OH + O. \tag{R$_8$}$$

The rate of reaction R_8 has a maximum around $z = 12$ km, a result of two competing processes (Fig. 4c). Above $z = 8$ km, the HO_2 concentration decreases with increasing altitude (Fig. 5a), whereas below $z = 24$ km, the rate coefficient of reaction R_8 increases with increasing altitude due to absorption and scattering of the incoming UV-radiation. A minor contribution to the global CO_2-production is

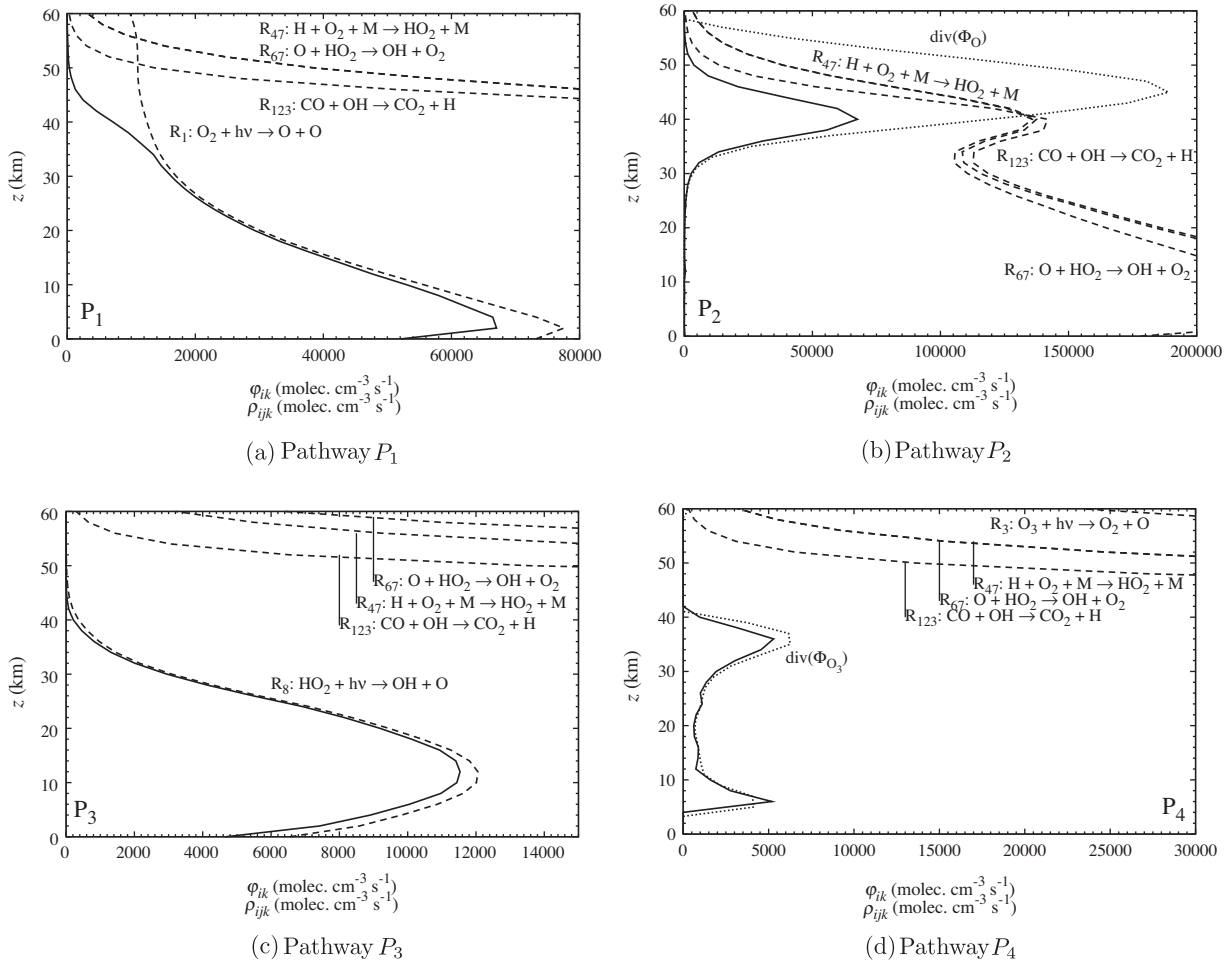

Fig. 4. Altitude-dependencies of rates associated with pathways P_1–P_4. The solid lines indicate the rates of CO_2-production by pathways P_1–P_4 (φ_{ik} from Eq. (9) with $S_i = CO_2$, P_k as indicated). Dashed lines mark the constraints on the CO_2-production rates of pathways P_1–P_4 imposed by individual reactions (ρ_{ijk} from Eq. (11) with $S_i = CO_2$, P_k, R_j indicated in the figure). Note that in the upper left and lower right panels, the ρ_{ijk} for R_{47} and R_{67} overlie. In the lower left panel the ρ_{ijk} for $R_j = R_{47}$ and with $R_j = R_{67}$ do not overlie, since R_{47} occurs twice in pathway P_3, but only once in reaction R_{67}. In the right panels, the dotted lines indicate the contribution of atomic oxygen by diffusion.

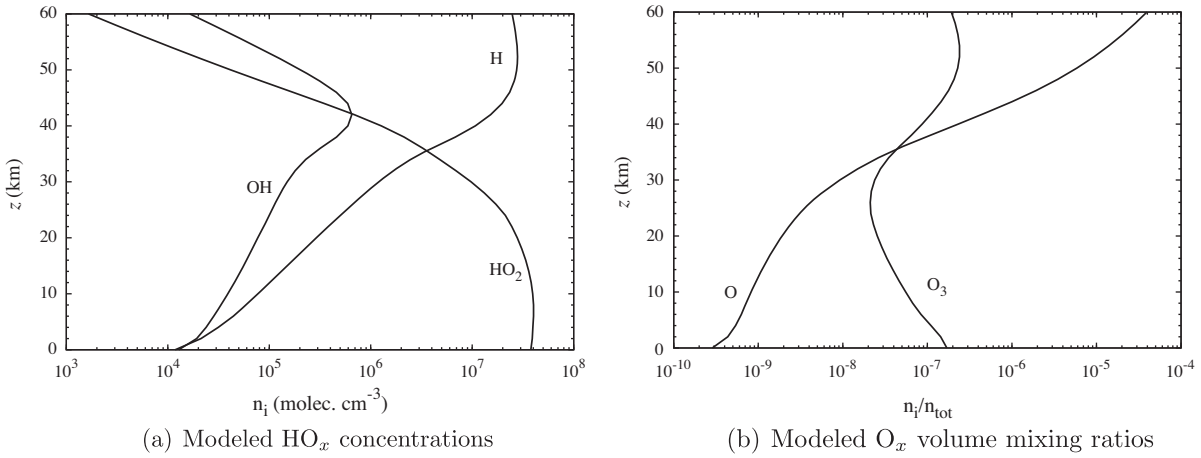

Fig. 5. Modeled concentrations of the species H, OH and HO_2 and volume mixing ratio altitude profiles of the species O and O_3. n_{tot} denotes the total number density of the atmosphere at given altitude z.

made by pathway P_4. This pathway is completely limited by the supply of ozone due to vertical transport (Fig. 4d). Its rate has two distinct clear cut maxima at $z = 6$ km and $z = 36$ km. The upper maximum depends on the downward transport of ozone from upper layers. The lower maximum originates from the upward transport of ozone from the lower layers (Fig. 5b).

3.1.2. Class Ib

The remaining two O_x–HO_x-pathways, P_5 and P_6 (Table 3), are variations of scheme Ib presented by Yung and DeMore (1999). For pathway P_5, atomic oxygen is supplied by downward transport from the upper atmosphere. However, in this case, the oxygen transport is not the limiting factor, since in the part of the atmosphere where pathway P_5 has its maximum rate, sufficient atomic oxygen is provided by transport (Fig. 6a). For altitudes between $z = 30$ km and $z = 45$ km, the rate of pathway P_5 is bounded from above by the O_2-formation reaction R_{52}. The majority of OH produced by reaction R_{52} and not consumed by pathway P_5 is either trapped in the null pathway P_{13} or used for O_2-production via

$$\begin{aligned} &O + OH \rightarrow O_2 + H \\ &H + O_3 \rightarrow OH + O_2 \\ &O + O_2 + CO_2 \rightarrow O_3 + CO_2 \\ &\text{net}: \quad 2O \rightarrow O_2. \end{aligned} \tag{P16}$$

Table 4
Class II HO_x-pathway percentage-contribution to the global CO_2-production by all CO_2-production-pathways. Values on the right hand side are calculated according to Eq. (17).

P_7	$H_2O_2 + h\nu \rightarrow OH + OH$ $2 \cdot (CO + OH \rightarrow CO_2 + H)$ $2 \cdot (H + O_2 + M \rightarrow HO_2 + M)$ $HO_2 + HO_2 \rightarrow H_2O_2 + O_2$	
net:	$2CO + O_2 \rightarrow 2CO_2$	**8.2%**
P_8	$H + HO_2 \rightarrow OH + OH$ $2 \cdot (CO + OH \rightarrow CO_2 + H)$ $H + O_2 + M \rightarrow HO_2 + M$	
net:	$2CO + O_2 \rightarrow 2CO_2$	**1.4%**

At higher altitudes, i.e. $z \geqslant 45$ km, the reaction with the smallest rate occurring in pathway P_5 is the CO_2-formation reaction R_{123}. Atomic hydrogen produced by this reaction is mainly involved in CO_2-production by pathways P_2 and P_5.

The difference between pathways P_5 and P_6 is the source of atomic oxygen. While the atomic oxygen in pathway P_5 comes from the upper atmosphere by transport, in case of pathway P_6 the atomic oxygen is produced by the O_2-photolysis reaction R_1 (Table 3). There are three regions, where $f_6^{max}(z)$ is determined by three different reactions (Fig. 6b). Below $z = 34$ km it is reaction

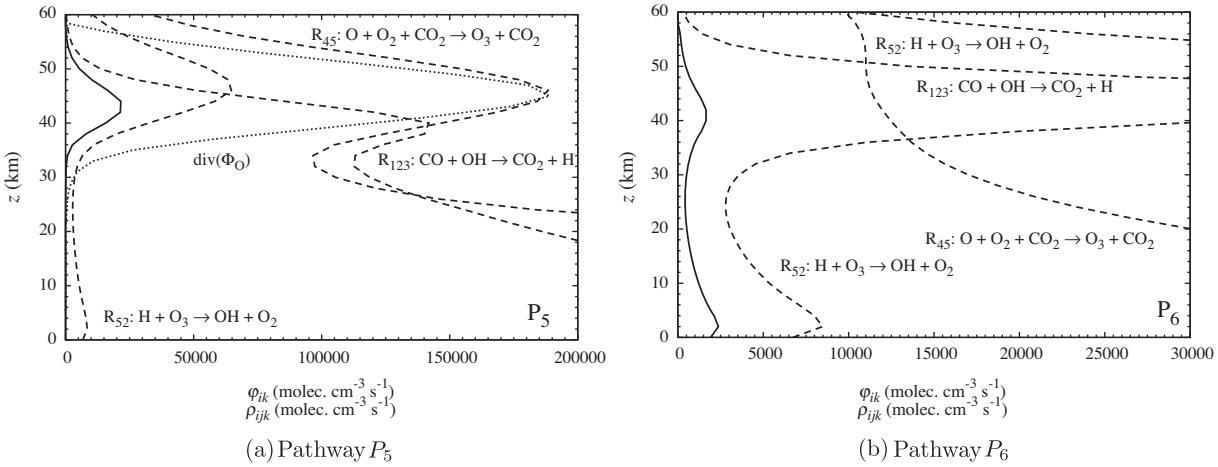

Fig. 6. Altitude-dependencies of rates associated with pathways P_5 and P_6. The solid lines indicate the rates of CO_2-production by pathways P_5 and P_6 (φ_{ik} from Eq. (9) with $S_i = CO_2$, P_k as indicated). Dashed lines mark the constraints on the CO_2-production rate of pathways P_5 and P_6 imposed by individual reactions (ρ_{ijk} from Eq. (11) with $S_i = CO_2$. P_k and R_j indicated in the figure). In the left panel, the dotted line indicates the contribution of atomic oxygen by diffusion.

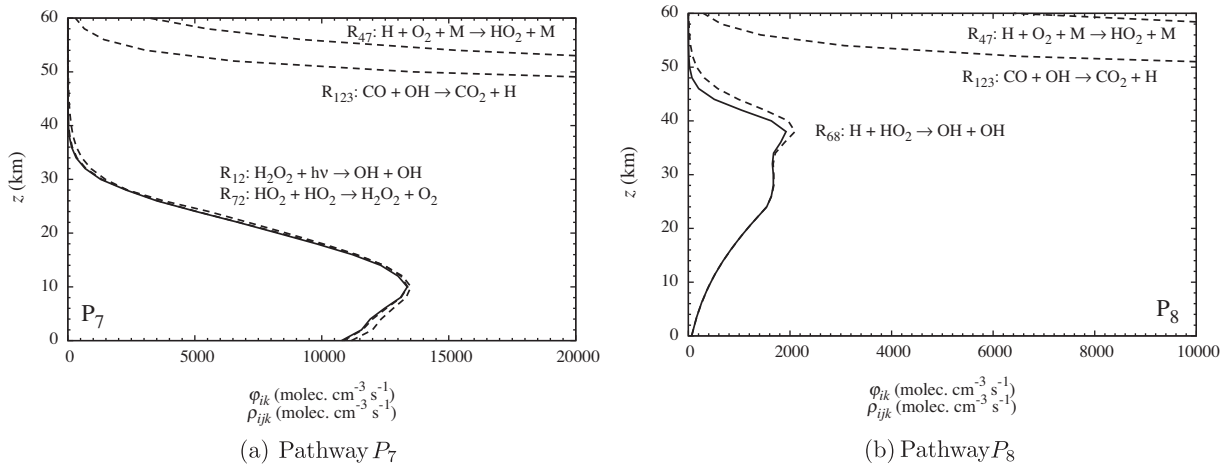

Fig. 7. Altitude-dependencies of rates associated with pathways P_7 and P_8. The solid lines indicate the rates of CO_2-production by pathway P_7 and P_8 (φ_{ik} from Eq. (9) with $S_i = CO_2$. P_k as indicated). Dashed lines mark the constraints on the CO_2-production rates of pathway P_7 and P_8 imposed by individual reactions (ρ_{ijk} from Eq. (11) with $S_i = CO_2$, P_k and R_j indicated in the figure). Note that in the left panel the reaction rates of R_{12} and R_{72} overlie.

Table 5
Class III O_x-HO_x-NO_x-pathway percentage-contribution to the global CO_2-production by all CO_2-production-pathways. Values on the right are calculated according to Eq. (17).

P_9	$NO + HO_2 \rightarrow NO_2 + OH$ $NO_2 + h\nu \rightarrow NO + O$ $O + HO_2 \rightarrow OH + O_2$ $2 \cdot (CO + OH \rightarrow CO_2 + H)$ $2 \cdot (H + O_2 + M \rightarrow HO_2 + M)$	
net:	$2CO + O_2 \rightarrow 2CO_2$	**10.3%**

R_{52}, between $z = 34$ km and $z = 52$ km it is the termolecular ozone formation reaction

$$O + O_2 + CO_2 \rightarrow O_3 + CO_2, \qquad (R_{45})$$

and above $z = 52$ km, the decisive reaction is R_{123}. In the lower regime, OH produced by reaction R_{52} is mainly consumed by the null pathway P_{13}. Between lower and upper regimes, most of O_3 produced by reaction R_{45} is directly photolyzed. This process results in the null pathway

$$O_3 + h\nu \rightarrow O_2 + O,$$
$$O + O_2 + CO_2 \rightarrow O_3 + CO_2,$$
$$\text{net}: \quad \text{null}. \qquad (P_{17})$$

In the upper regime, only a fraction of the hydrogen amount produced by reaction R_{123} is consumed by pathway P_6. The remaining H is predominantly used either by pathway P_5 or the null pathway P_{13}. A distinctive feature of this pathway is that its actual rate $f_6(z)$ is significantly smaller than its potential maximum rate $f_6^{max}(z)$. This means, that the branching-point species produced by reactions involved in pathway P_6 are efficiently consumed by competing pathways.

Since P_1 and P_2 (and also P_6 and P_5) differ only by the O_2-photolysis reaction R_1, therefore the ratio $\varphi_{i1}(z)/\varphi_{i2}(z)$ equals the ratio $\varphi_{i6}(z)/\varphi_{i5}(z)$ for $S_i = CO_2$ at each altitude z. However, the ratio of the globally-averaged rates q_{i1}/q_{i2} is larger than the ratio q_{i6}/q_{i5}. This is a consequence of the decrease of $\varphi_{i1}/\varphi_{i2} = \varphi_{i6}/\varphi_{i5}$ for increasing altitude z (see Fig. 3) in combination with different altitude dependence of the rates of the individual pathways.

3.2. Class II: HO_x-pathways

The second class of pathways (here P_7 and P_8, see Table 4) consists of HO_x-pathways, which have no reactions including O or O_3. In pathway P_7, OH is formed by the photo-dissociation of hydrogen peroxide via

$$H_2O_2 + h\nu \rightarrow OH + OH. \qquad (R_{12})$$

The pathway P_7 was previously introduced by Parkinson and Hunten (1972). The rate of pathway P_7 is restricted by reactions R_{12} and

$$HO_2 + HO_2 \rightarrow H_2O_2 + O_2, \qquad (R_{72})$$

where the latter produces H_2O_2, which is subsequently photolyzed via reaction R_{12} (Fig. 7a). Pathway P_8, proposed by Sonnemann et al. (2006), has only a minor contribution to the global CO_2-production. Its rate $f_8(z)$ is basically limited by the reaction

$$H + HO_2 \rightarrow OH + OH. \qquad (R_{68})$$

The reaction rate of R_{68} is characterized by an increase of the concentration of H and a decrease of the concentration of HO_2 with altitude (Figs. 5a and 7b).

3.3. Class III: O_x–HO_x–NO_x-pathways

The third class of dominant chemical pathways in this study contains only one pathway, namely P_9 (see Table 5), which includes additional species from the NO_x-family as catalysts. This pathway is especially important at altitudes below $z = 30$ km (Fig. 8). There, f_k^{max} is determined by the rate $r_{17}(z)$ of NO_2-photolysis

$$NO_2 + h\nu \rightarrow NO + O. \qquad (R_{17})$$

Below $z = 12$ km NO and O, which are produced by this reaction and not consumed by P_9 are mainly trapped in the null pathways

$$NO_2 + h\nu \rightarrow NO + O,$$
$$O_3 + NO \rightarrow NO_2 + O_2,$$
$$O + O_2 + CO_2 \rightarrow O_3 + CO_2,$$
$$\text{net}: \quad \text{null}, \qquad (P_{18})$$

and

$$NO_2 + h\nu \rightarrow NO + O,$$
$$O + NO + M \rightarrow NO_2 + M,$$
$$\text{net}: \quad \text{null}. \qquad (P_{19})$$

3.4. Global contribution of CO_2-production-pathways

The global relative contribution of the individual CO_2-production-pathways to the total CO_2-production by chemical pathways

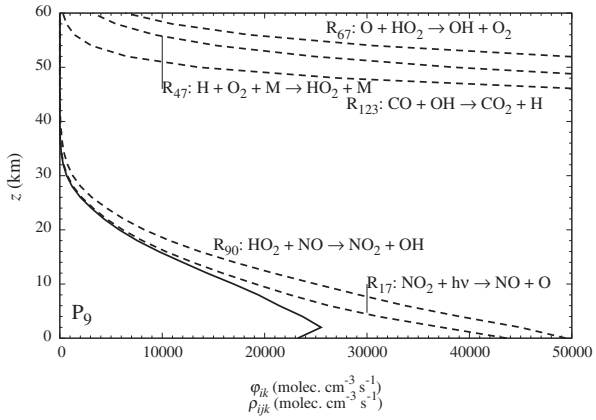

Fig. 8. Altitude-dependence of rates associated with pathway P_9. The solid line indicates the rate of CO_2-production by pathway P_9 (φ_{ik} from Eq. (9) with $S_i = CO_2$, $P_k = P_9$). Dashed lines show the constraints on the rate of CO_2-production by pathway P_9 imposed by individual reactions (ρ_{ijk} from Eq. (11) with $S_i = CO_2$, $P_k = P_9$, R_j indicated in the figure). Note that ρ_{ijk} with $R_j = R_{47}$ and ρ_{ijk} with $R_j = R_{67}$ do not lie on top of each other, since R_{47} occurs twice in pathway P_9, but R_{67} only once.

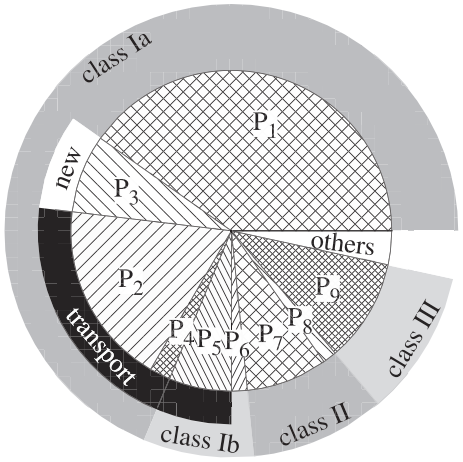

Fig. 9. Contribution of chemical pathways to the global CO_2-production calculated according to Eq. (17). The inner circular disk shows the relative contributions of the individual pathways to the global CO_2-production. Numerical values are given in the corresponding Tables 2 and 5. The outer ring points to which class the individual pathways belong. The black circular ring segment indicates chemical pathways which require O_x by vertical transport. Pathways, previously not reported in the literature, are marked "new".

q_{ik} is calculated using Eq. (17). Fig. 9 shows the nine dominant pathways which account for more than 96% of the CO_2-production. The largest contribution is thereby made by O_x–HO_x-pathways (76.6%), followed by the O_x–HO_x–NO_x-pathways (10.4%), and O_x–HO_x-pathways (9.6%). The remaining 3.4% are produced by summing a large number of pathways, which have only a minor contribution. These pathways occur especially in the lower layers of the atmosphere (see Fig. 3), where NO_x-chemistry becomes more important. Pathways which depend on the vertical transport of either atomic oxygen or ozone have a contribution of 26.9%. This suggests that transport processes have a significant impact on CO_2-production and hence the photochemical stability of the Martian atmosphere.

3.5. Uncertainties

All input parameters required by photochemical models (e.g. photochemical absorption cross-sections, reaction rate coefficients, eddy-diffusion profiles, etc.) are clearly only known within a certain range of uncertainty. These uncertainties can affect the time-averaged concentrations $\langle n_i \rangle(z)$ of chemical species as well as the time-averaged chemical reaction rates $\langle r_j \rangle(z)$ which in turn can influence the results of the pathway analysis. The same is also true for numerical uncertainties. However, numerical errors are negligible in comparison to the uncertainties in the input parameters.

To investigate the effect of the above uncertainties on the results of the pathway analysis, a comprehensive global sensitivity analysis would be required in order to account for the non-linear behavior of the modeled atmosphere. Such an analysis would require a large number of simulations to obtain statistically relevant results and highly sophisticated numerical techniques to identify the key-uncertainties (Dobrijevic et al., 2010) and is therefore beyond the scope of this paper.

Nevertheless, the identification of the dominant pathways can give an indication of those chemical reactions, which have a significant influence on the CO_2 abundance as calculated by the Caltech/JPL photochemical column model. Out of 126 reactions, only 13 participate in the nine dominant CO_2-production-pathways P_1–P_9 (see A.1). Whereas sensitivity analysis methods can pinpoint key-reactions which strongly impact the numerical solutions of photochemical models, PAP provides information regarding the interrelationship between chemical reactions. The pathway analysis of chemical reaction networks can therefore be regarded as complementary to standard sensitivity analysis methods. Combined pathway and sensitivity analyses will be the subject of future studies.

3.6. Impact of potentially missing trace species and reactions

The PAP algorithm identifies all significant pathways in a *given* reaction system. Trace gas species or reactions not included can therefore not be detected by this algorithm.

For example, a species which is present on Mars, but not part of the reaction scheme is ^{40}Ar (Owen et al., 1977). Being a noble-gas, ^{40}Ar is chemically inactive and does not take part in chemical gas-phase reactions. Therefore, the outcome of the pathway analysis will not be affected by neglecting ^{40}Ar in the chemical scheme.

More interesting effects are expected by adding more reactive species, like the activated complex $HOCO^{\ddagger}$ to the reaction network. $HOCO^{\ddagger}$, can be formed via

$$CO + OH \rightarrow HOCO^{\ddagger}, \qquad (R_{123a})$$

and can react further to

$$HOCO^{\ddagger} \rightarrow CO_2 + H \qquad (R_{123b})$$

(Smith and Zellner, 1973; Senosiain et al., 2003), replacing reaction R_{123}. If $HOCO^{\ddagger}$ decomposes into the products given by reaction R_{123b} before it can react with other species, no significant changes, except the separation of reaction R_{123} into two parts (reactions R_{123a} and R_{123b}), will be seen in the identified pathways. Significant changes might occur if $HOCO^{\ddagger}$ can be thermally stabilized

$$HOCO^{\ddagger} + M \rightarrow HOCO + M. \qquad (R_{123c})$$

In this case the probability for HOCO taking part in bimolecular reactions becomes more probable, forming potentially new pathways (Boxe et al., 2010). The role for the Martian atmospheric chemistry of potentially missing species and reactions can be investigated by expanding the current scheme used in the Caltech/JPL photochemical column model presupposing reaction rate coefficients are known or can be estimated. The PAP-algorithm can then be used again to assess the relevance of newly added species and reactions in relation to the existing well-established reaction network.

4. Summary and conclusions

In order to address the CO_2 stability problem of the Martian atmosphere, we have applied for the first time the *Pathway Analysis Program* (PAP) to the modified Caltech/JPL photochemical column model of the Martian atmosphere. All dominant CO_2-production-pathways in the underlying reaction network throughout the lower to middle atmosphere, where CO_2-production is efficient, have been identified and quantified. Our results are in good agreement with previous studies (e.g. McElroy and Donahue, 1972; Parkinson and Hunten, 1972; Yung and DeMore, 1999) which proposed the most dominant pathways involving HO_x and NO_x respectively. The algorithm was also capable to identify pathways with minor contributions, e.g. P_8 (Sonnemann et al., 2006). In addition, we have calculated relative contributions of chemical pathways to the global CO_2-production in Mars' atmosphere. Our results indicate that only nine pathways account for 96.6% of the global CO_2-production. The pathways found can be categorized into three classes (class I: O_x–HO_x-pathways, class II: HO_x-pathways, and class III: O_x–HO_x–NO_x-pathways) according to key molecules occurring in the pathways. In order to gain more insight into class I pathways, it is advantageous to split this group into smaller sub-classes, which account for the different fate of atomic hydrogen. The global CO_2-production is dominated by O_x–HO_x-pathways. Nevertheless O_x–HO_x–NO_x-pathways have a substantial effect on the CO_2-production, especially at lower altitudes. Among the nine dominant pathways, we discovered a new chemical pathway, involving HO_2-photolysis, which contributes approximately 8% towards global CO_2-production. We have calculated pathway rates as functions of altitude, whereby the efficiency of individual pathways varies drastically with altitude. Furthermore, our investigations revealed that in some cases a significant discrepancy between the actual rate of a pathway $f_k(z)$ and its potential maximum rate $f_k^{\max}(z)$ can occur. This phenomenon is a consequence of the competition between pathways, which also has been determined in this study. Almost 27% of CO_2-production is due to chemical pathways, which consume the species O or O_3. These have a relatively short lifetime in comparison to the time-scale of CO–CO_2-interconversion and are provided by vertical transport. This in turn indicates a close coupling between dynamical and chemical processes in the Martian atmosphere. The study is the first to quantify the contribution of specific chemical pathways towards the overall stability of the atmosphere. Therefore results herein provide deeper insights towards the role of trace gases being measured by future missions like, e.g. the ExoMars Trace Gas Orbiter (Witasse and Allen, 2011).

Acknowledgment

This research has been partly supported by the Helmholtz Association through the research alliance "Planetary Evolution and Life".

Appendix A. Chemical reactions in the Caltech/JPL Mars atmosphere model

See Table A1.

Table A1
Chemical reactions in the Caltech/JPL model Mars atmosphere. All reactions are updated according to Sander et al. (2006). Rate coefficients are given in s^{-1} for unimolecular reactions, cm^3 $molec.^{-1}$ s^{-1} for bimolecular reactions, and cm^6 $molec.^{-2}$ s^{-1} for termolecular reactions. For photolysis reactions, rate coefficients are given at the lower (0 km) and upper boundary (240 km) of the model. For three-body reactions, lower (k_0) and upper (k_∞) pressure limits are given. Reactions, which occur in the nine dominant pathways, are marked with a bullet (•).

		Reaction	Rate coefficient
•	R_1	$O_2 + h\nu \rightarrow O + O$	1.0×10^{-10}, 2.2×10^{-7}
	R_2	$O_2 + h\nu \rightarrow O + O(^1D)$	0, 5.5×10^{-7}
•	R_3	$O_3 + h\nu \rightarrow O_2 + O$	1.9×10^{-4}, 3.8×10^{-4}
	R_4	$O_3 + h\nu \rightarrow O_2 + O(^1D)$	4.3×10^{-7}, 9.6×10^{-7}
	R_5	$O_3 + h\nu \rightarrow O + O + O$	1.1×10^{-10}, 9.8×10^{-7}
	R_6	$H_2 + h\nu \rightarrow H + H$	0, 7.3×10^{-8}
	R_7	$OH + h\nu \rightarrow O + H$	2.7×10^{-18}, 3.0×10^{-6}
•	R_8	$HO_2 + h\nu \rightarrow OH + O$	8.7×10^{-5}, 1.7×10^{-4}
	R_9	$H_2O + h\nu \rightarrow H + OH$	1.9×10^{-12}, 2.0×10^{-6}
	R_{10}	$H_2O + h\nu \rightarrow H_2 + O(^1D)$	0, 1.1×10^{-7}
	R_{11}	$H_2O + h\nu \rightarrow H + H + O$	0, 1.2×10^{-7}
•	R_{12}	$H_2O_2 + h\nu \rightarrow OH + OH$	1.4×10^{-5}, 3.2×10^{-5}
	R_{13}	$N_2 + h\nu \rightarrow N + N(^2D)$	0, 0
	R_{14}	$N_2 + h\nu \rightarrow N + N$	0, 1.9×10^{-7}
	R_{15}	$N_2 + h\nu \rightarrow N(^2D) + N(^2D)$	0, 0
	R_{16}	$NO + h\nu \rightarrow N + O$	1.7×10^{-17}, 1.2×10^{-6}
•	R_{17}	$NO_2 + h\nu \rightarrow NO + O$	1.6×10^{-3}, 2.6×10^{-3}
	R_{18}	$NO_3 + h\nu \rightarrow NO_2 + O$	3.0×10^{-2}, 5.2×10^{-2}
	R_{19}	$NO_3 + h\nu \rightarrow NO + O_2$	4.4×10^{-3}, 6.0×10^{-3}
	R_{20}	$N_2O + h\nu \rightarrow N_2 + O(^1D)$	3.0×10^{-8}, 1.0×10^{-6}
	R_{21}	$N_2O_5 + h\nu \rightarrow NO_2 + NO_3$	3.6×10^{-5}, 6.8×10^{-5}
	R_{22}	$N_2O_5 + h\nu \rightarrow NO + NO_3 + O$	6.9×10^{-5}, 1.4×10^{-4}
	R_{23}	$HNO_2 + h\nu \rightarrow OH + NO$	3.5×10^{-4}, 5.8×10^{-4}
	R_{24}	$HNO_3 + h\nu \rightarrow NO_2 + OH$	9.9×10^{-6}, 4.0×10^{-5}
	R_{25}	$HO_2NO_2 + h\nu \rightarrow HO_2 + NO_2$	4.1×10^{-5}, 9.2×10^{-5}
	R_{26}	$HO_2NO_2 + h\nu \rightarrow OH + NO_3$	2.2×10^{-5}, 5.0×10^{-5}
	R_{27}	$CO_2 + h\nu \rightarrow CO + O$	7.6×10^{-13}, 3.8×10^{-9}
	R_{28}	$CO_2 + h\nu \rightarrow CO + O(^1D)$	0, 1.1×10^{-7}
	R_{29}	$O + M \rightarrow O^+ + e^- + M$	0, 4.7×10^{-8}
	R_{30}	$O_2 + h\nu \rightarrow O_2^+ + e^-$	0, 1.6×10^{-7}
	R_{31}	$CO_2 + h\nu \rightarrow CO_2^+ + e^-$	0, 2.0×10^{-7}
	R_{32}	$CO_2 + h\nu \rightarrow CO + O^+ + e^-$	0, 1.1×10^{-8}
	R_{33}	$O_2^+ + e^- \rightarrow O + O$	$6.6 \times 10^{-5} T^{-1.0}$

Table A1 (*continued*)

		Reaction	Rate coefficient
	R_{34}	$CO_2^+ + e^- \rightarrow CO + O$	3.8×10^{-7}
	R_{35}	$CO_2H^+ + e^- \rightarrow CO_2 + H$	3.0×10^{-7}
	R_{36}	$O^+ + CO_2 \rightarrow O_2^+ + CO$	9.6×10^{-10}
	R_{37}	$O(^1D) + O_2 \rightarrow O + O_2$	$3.2 \times 10^{-11} e^{70/T}$
	R_{38}	$O(^1D) + N_2 \rightarrow O + N_2$	$1.8 \times 10^{-11} e^{110/T}$
	R_{39}	$O(^1D) + CO_2 \rightarrow O + CO_2$	$7.4 \times 10^{-11} e^{120/T}$
	R_{40}	$O + O + M \rightarrow O_2 + M$	$5.21 \times 10^{-35} e^{900/T}$
	R_{41}	$O + O + O_2 \rightarrow O_3 + O$	$k_0 = 5.9 \times 10^{-34}(T/300)^{-2.4}$ $k_\infty = 2.8 \times 10^{-12}$
	R_{42}	$O + O_2 + O_2 \rightarrow O_3 + O_2$	$k_0 = 5.9 \times 10^{-34}(T/300)^{-2.4}$ $k_\infty = 2.8 \times 10^{-12}$
	R_{43}	$O + O_2 + N_2 \rightarrow O_3 + N_2$	$5.95 \times 10^{-34}(T/300)^{-2.3}$
	R_{44}	$O + O_2 + CO \rightarrow O_3 + CO$	$k_0 = 6.7 \times 10^{-34}(T/300)^{-2.5})$ $k_\infty = 2.8 \times 10^{-12}$
•	R_{45}	$O + O_2 + CO_2 \rightarrow O_3 + CO_2$	$5.0 \times 10^{-35} e^{724/T}$
	R_{46}	$O + O_2 + M \rightarrow O_3 + M$	$6.0 \times 10^{-34}(T/300)^{-2.4}$
•	R_{47}	$H + O_2 + M \rightarrow HO_2 + M$	$k_0 = 5.7^{-32}(T/300)^{-1.6}$ $k_\infty = 7.5 \times 10^{-11}$
	R_{48}	$N + O_2 \rightarrow NO + O$	$1.5 \times 10^{-11} e^{-3600/T}$
	R_{49}	$O + O_3 \rightarrow O_2 + O_2$	$8.0 \times 10^{-12} e^{-2060/T}$
	R_{50}	$O(^1D) + O_3 \rightarrow O_2 + O_2$	1.2×10^{-10}
	R_{51}	$O(^1D) + O_3 \rightarrow O + O + O_2$	1.2×10^{-10}
•	R_{52}	$H + O_3 \rightarrow OH + O_2$	$1.4 \times 10^{-10} e^{-470/T}$
	R_{53}	$OH + O_3 \rightarrow HO_2 + O_2$	$1.7 \times 10^{-12} e^{-940/T}$
	R_{54}	$HO_2 + O_3 \rightarrow OH + O_2 + O_2$	$1.0 \times 10^{-14} e^{-490/T}$
	R_{55}	$N + O_3 \rightarrow NO + O_2$	2.0×10^{-16}
	R_{56}	$O + H + M \rightarrow OH + M$	$1.3 \times 10^{-29} T^{-1.0}$
	R_{57}	$H + H + M \rightarrow H_2 + M$	$2.7 \times 10^{-31} T^{-0.6}$
	R_{58}	$O + H_2 \rightarrow OH + H$	$8.5 \times 10^{-20} T^{2.7} e^{-3160/T}$
	R_{59}	$O(^1D) + H_2 \rightarrow H + OH$	1.1×10^{-10}
	R_{60}	$OH + H_2 \rightarrow H_2O + H$	$5.5 \times 10^{-12} e^{-2000/T}$
	R_{61}	$O + OH \rightarrow O_2 + H$	$2.2 \times 10^{-11} e^{120/T}$
	R_{62}	$H + OH + N_2 \rightarrow H_2O + N_2$	$6.1 \times 10^{-26} T^{-2.0}$
	R_{63}	$H + OH + CO_2 \rightarrow H_2O + CO_2$	$7.7 \times 10^{-26} T^{-2.0}$
	R_{64}	$OH + OH \rightarrow H_2O + O$	$4.2 \times 10^{-12} e^{-240/T}$
	R_{65}	$N + OH \rightarrow NO + H$	$3.8 \times 10^{-11} e^{85/T}$
	R_{66}	$OH + OH + M \rightarrow H_2O_2 + M$	$k_0 = 6.2 \times 10^{-31}(T/300)^{-1.0}$ $k_\infty = 2.6 \times 10^{-11}$
•	R_{67}	$O + HO_2 \rightarrow OH + O_2$	$3.0 \times 10^{-11} e^{200/T}$
•	R_{68}	$H + HO_2 \rightarrow OH + OH$	7.21×10^{-11}
	R_{69}	$H + HO_2 \rightarrow H_2 + O_2$	7.29×10^{-12}
	R_{70}	$H + HO_2 \rightarrow H_2O + O$	1.62×10^{-12}
	R_{71}	$OH + HO_2 \rightarrow H_2O + O_2$	$3.2 \times 10^{-11} e^{450/T}$
•	R_{72}	$HO_2 + HO_2 \rightarrow H_2O_2 + O_2$	$2.3 \times 10^{-13} e^{600/T}$
	R_{73}	$HO_2 + HO_2 + M \rightarrow H_2O_2 + O_2 + M$	$1.7 \times 10^{-33} e^{1000/T}$
	R_{74}	$O(^1D) + H_2O \rightarrow OH + OH$	2.2×10^{-10}
	R_{75}	$O + H_2O_2 \rightarrow OH + HO_2$	$1.4 \times 10^{-12} e^{-2000/T}$
	R_{76}	$OH + H_2O_2 \rightarrow H_2O + HO_2$	$2.9 \times 10^{-12} e^{-160/T}$
	R_{77}	$N(^2D) + O \rightarrow N + O$	6.9×10^{-13}
	R_{78}	$N(^2D) + N_2 \rightarrow N + N_2$	1.7×10^{-14}
	R_{79}	$N(^2D) + NO \rightarrow N_2 + O$	6.9×10^{-11}
	R_{80}	$N(^2D) + CO \rightarrow N + CO$	1.7×10^{-12}
	R_{81}	$N(^2D) + CO_2 \rightarrow NO + CO$	3.5×10^{-13}
	R_{82}	$N + HO_2 \rightarrow NO + OH$	2.2×10^{-11}
	R_{83}	$N_2O_5 + H_2O \rightarrow HNO_3 + HNO_3$	2.0×10^{-21}
	R_{84}	$N + N + M \rightarrow N_2 + M$	$8.27 \times 10^{-34} e^{490/T}$
	R_{85}	$O(^1D) + N_2 + M \rightarrow N_2O + M$	$3.5 \times 10^{-37}(T/300)^{-0.6}$
	R_{86}	$N_2 \rightarrow N + N$	$0.0{,}2.7 \times 10^{-7}$
	R_{87}	$O + NO + M \rightarrow NO_2 + M$	$k_0 = 9.0 \times 10^{-31}(T/300)^{-1.5}$ $k_\infty = 3.0 \times 10^{-11}$
	R_{88}	$O_3 + NO \rightarrow NO_2 + O_2$	$3.0 \times 10^{-12} e^{-1500/T}$
	R_{89}	$OH + NO + M \rightarrow HNO_2 + M$	$k_0 = 7.0 \times 10^{-31}(T/300)^{-2.6}$ $k_\infty = 3.6 \times 10^{-11}(T/300)^{-0.1}$
•	R_{90}	$HO_2 + NO \rightarrow NO_2 + OH$	$3.5 \times 10^{-12} e^{250/T}$
	R_{91}	$N + NO \rightarrow N_2 + O$	$2.1 \times 10^{-11} e^{100/T}$
	R_{92}	$O + NO_2 \rightarrow NO + O_2$	$5.6 \times 10^{-12} e^{180/T}$
	R_{93}	$O + NO_2 + M \rightarrow NO_3 + M$	$k_0 = 2.5 \times 10^{-31}(T/300)^{-1.8}$ $k_\infty = 2.2 \times 10^{-11}(T/300)^{-0.7}$
	R_{94}	$O_3 + NO_2 \rightarrow NO_3 + O_2$	$1.2 \times 10^{-13} e^{-2450/T}$
	R_{95}	$H + NO_2 \rightarrow OH + NO$	$4.0 \times 10^{-10} e^{-340/T}$
	R_{96}	$OH + NO_2 + M \rightarrow HNO_3 + M$	$k_0 = 2.0 \times 10^{-30}(T/300)^{-3.0}$

(*continued on next page*)

Table A1 (*continued*)

	Reaction	Rate coefficient
		$k_\infty = 2.5 \times 10^{-11} e^{300/T}$
R_{97}	$HO_2 + NO_2 \rightarrow HNO_2 + O_2$	5.0×10^{-16}
R_{98}	$HO_2 + NO_2 + M \rightarrow HO_2NO_2 + M$	$k_0 = 1.8 \times 10^{-31}(T/300)^{-3.2}$
		$k_\infty = 4.7 \times 10^{-12}(T/300)^{-1.4}$
R_{99}	$N + NO_2 \rightarrow N_2O + O$	$5.8 \times 10^{-12} e^{220/T}$
R_{100}	$NO_3 + NO_2 \rightarrow NO + NO_2 + O_2$	$4.5 \times 10^{-14} e^{-1260/T}$
R_{101}	$NO_3 + NO_2 + M \rightarrow N_2O_5 + M$	$k_0 = 2.0 \times 10^{-30}(T/300)^{-4.4}$
		$k_\infty = 1.4 \times 10^{-12}(T/300)^{-0.7}$
R_{102}	$O + NO_3 \rightarrow O_2 + NO_2$	1.0×10^{-11}
R_{103}	$H + NO_3 \rightarrow OH + NO_2$	1.1×10^{-10}
R_{104}	$OH + NO_3 \rightarrow HO_2 + NO_2$	2.2×10^{-11}
R_{105}	$HO_2 + NO_3 \rightarrow HNO_3 + O_2$	3.5×10^{-12}
R_{106}	$NO + NO_3 \rightarrow NO_2 + NO_2$	$1.5 \times 10^{-11} e^{170/T}$
R_{107}	$NO_3 + NO_3 \rightarrow NO_2 + NO_2 + O_2$	$8.5 \times 10^{-13} e^{-2450/T}$
R_{108}	$CO + NO_3 \rightarrow NO_2 + CO_2$	4.0×10^{-19}
R_{109}	$O(^1D) + N_2O \rightarrow NO + NO$	6.7×10^{-11}
R_{110}	$O(^1D) + N_2O \rightarrow N_2 + O_2$	4.9×10^{-11}
R_{111}	$O + N_2O_5 \rightarrow NO_2 + NO_2 + O_2$	3.0×10^{-16}
R_{112}	$N_2O_5 + M \rightarrow NO_3 + NO_2 + M$	$6.0 \times 10^{-4} T^{-4.4} e^{-10990/T}$
R_{113}	$O_3 + HNO_2 \rightarrow O_2 + HNO_3$	5.0×10^{-19}
R_{114}	$OH + HNO_2 \rightarrow H_2O + NO_2$	$1.8 \times 10^{-11} e^{-390/T}$
R_{115}	$O + HNO_3 \rightarrow OH + NO_3$	3.0×10^{-17}
R_{116}	$OH + HNO_3 \rightarrow NO_3 + H_2O$	$7.2 \times 10^{-15} e^{785/T}$
R_{117}	$O + HO_2NO_2 \rightarrow OH + NO_2 + O_2$	$7.8 \times 10^{-11} e^{-3400/T}$
R_{118}	$OH + HO_2NO_2 \rightarrow H_2O + NO_2 + O_2$	$1.3 \times 10^{-12} e^{380/T}$
R_{119}	$HO_2NO_2 + M \rightarrow HO_2 + NO_2 + M$	$8.57 \times 10^{-5} T^{-3.2} e^{-10900/T}$
R_{120}	$O + CO + M \rightarrow CO_2 + M$	$k_0 = 1.7 \times 10^{-33} e^{-1510/T}$
		$k_\infty = 2.66 \times 10^{-14} e^{-1459/T}$
R_{121}	$O + CO + CO \rightarrow CO_2 + CO$	$6.5 \times 10^{-33} e^{-2180/T}$
R_{122}	$O + O + CO \rightarrow CO_2 + O$	$3.40 \times 10^{-33} e^{-2180/T}$
• R_{123}	$OH + CO \rightarrow CO_2 + H$	$3.2 \times 10^{-13} e^{-300/T}$
R_{124}	$CO_2^+ + O \rightarrow O_2^+ + CO$	1.64×10^{-10}
R_{125}	$CO_2^+ + O \rightarrow O^+ + CO_2$	9.62×10^{-11}
R_{126}	$CO_2^+ + H_2 \rightarrow CO_2H^+ + H$	4.7×10^{-10}

References

Anbar, A.D., Leu, M.-T., Nair, H.A., Yung, Y.L., 1993. Adsorption of HO_x on aerosol surfaces: Implications for the atmosphere of Mars. J. Geophys. Res. 98, 10933–10940.

Atreya, S.K., Gu, Z.G., 1994. Stability of the martian atmosphere: Is heterogeneous catalysis essential? J. Geophys. Res. 99, 13133–13145.

Boxe, C.S., Francisco, J.S., Shia, R.-L., Yung, Y.L., Liang, M.-C., Sander, S.P., Nair, H., Saiz-Lopez, A., 2012. New insights into martian atmospheric chemistry. Icarus, submitted for publication.

Clarke, B.L., 1988. Stoichiometric network analysis. Cell Biophys. 12, 237–253.

Dobrijevic, M., Hébrard, E., Plessis, S., Carrasco, N., Pernot, P., Bruno-Claeys, M., 2010. Comparison of methods for the determination of key reactions in chemical systems: Application to Titan's atmosphere. Adv. Space Res. 45, 77–91.

Grenfell, J.L., Lehmann, R., Mieth, P., Langematz, U., Steil, B., 2006. Chemical reaction pathways affecting stratospheric and mesospheric ozone. J. Geophys. Res. 111, D17311.

Johnston, H., Kinnison, D., 1998. Methane photooxidation in the atmosphere: Contrast between two methods of analysis. J. Geophys. Res. 103, 21967–21984.

Krasnopolsky, V.A., 1993. Photochemistry of the martian atmosphere (mean conditions). Icarus 101, 313–332.

Lehmann, R., 2004. An algorithm for the determination of all significant pathways in chemical reaction systems. J. Atmos. Chem. 47, 45–78.

Lefèvre, F. et al., 2008. Heterogeneous chemistry in the atmosphere of Mars. Nature 454, 971–975.

McElroy, M.B., Donahue, T.M., 1972. Stability of the martian atmosphere. Science 177, 986–988.

Milner, P.C., 1964. The possible mechanisms of complex reactions involving consecutive steps. J. Electrochem. Soc. 111, 228–232.

Nair, H., Allen, M., Anbar, A.D., Yung, Y.L., 1994. A photochemical model of the martian atmosphere. Icarus 111, 124–150.

Owen, T., Biemann, K., Rushneck, D.R., Biller, J.E., Howarth, D.W., Lafleur, A.L., 1977. The composition of the atmosphere at the surface of Mars. J. Geophys. Res. 82, 4369–4635.

Parkinson, T.M., Hunten, D.M., 1972. Spectroscopy and aeronomy of O_2 on Mars. J. Atmos. Sci. 29, 1380–1390.

Rabitz, H., Kramer, M., Dacol, D., 1983. Sensitivity analysis in chemical kinetics. Annu. Rev. Phys. Chem. 34, 419–461.

Saltelli, A., Ratto, M., Tarantola, S., Campolongo, F., 2005. Sensitivity analysis for chemical models. Chem. Rev. 105, 2811–2827.

Sander, S.P. et al., 2006. Chemical Kinetics and Photochemical Data for Use in Atmospheric Studies, Evaluation Number 15, JPL Publ., 06-2.

Schuster, R., Schuster, S., 1993. Refined algorithm and computer program for calculating all nonnegative fluxes admissible in steady states of biochemical reaction systems with or without some flux rates fixed. Comput. Appl. Biosci. 9, 79–85.

Senosiain, J.P., Musgrave, C.B., Golden, D.M., 2003. Temperature and pressure dependence of the reaction of OH and CO: Master equation modeling on a high-level potential energy surface. Int. J. Chem. Kinet. 35, 464–474.

Smith, I.W.M., Zellner, R., 1973. Rate measurements of reactions of OH by resonance absorption: Part 2 – Reactions of OH with CO, C_2H_4 and C_2H_2. J. Chem. Soc., Faraday Trans. 2 (69), 1617–1627.

Sonnemann, G.R., Hartogh, P., Medvedev, A.S., Grygalashvyly, M., Berger, U., 2006. A new coupled 3D-model of the dynamics and chemistry of the martian atmosphere and some problems of the chemical modeling. In: Forget, F. et al. (Eds.), Mars Atmospheric Modelling and Observations. LMD, IAA, AOPP, CNES, ESA, pp. 516–519.

Stock, J.W., Grenfell, J.L., Lehmann, R., Patzer, A.B.C., Rauer, H., 2011. Chemical pathway analysis of the lower martian atmosphere: The CO_2 stability problem. Planet. Space Sci., in press.

Turányi, T., 1990. Sensitivity analysis of complex kinetic systems. Tools and applications. J. Math. Chem. 5, 203–248.

Verronen, P.T., Santee, M.L., Manney, G.L., Lehmann, R., Salmi, S.-M., Seppälä, A., 2011. Nitric acid enhancements in the mesosphere during January 2005 and December 2006 solar proton events. J. Geophys. Res. 116, D17301.

Witasse, O., Allen, M., 2011. The ExoMars 2016 Trace Gas Orbiter. In: Forget, F., Millour, E. (Eds.), The Fourth International Workshop on the Mars Atmosphere: Modelling and Observation, 8-11 February, 2011, Paris, France, p. 479. Available from: <http://www-mars.lmd.jussieu.fr/paris2011/program.html>.

Yung, Y.L., DeMore, W.B., 1999. Photochemistry of Planetary Atmospheres. Oxford University Press, New York.

Yung, Y.L., Wen, J.S., Pinto, J.P., Allen, M., Pierce, K.K., Paulson, S., 1988. HDO in the martian atmosphere: Implications for the abundance of crustal water. Icarus 76, 146–159.